



A comparative study on the structural, optical, and electrical properties of titania films grown by spin-coating method

Akshayakumar Kompa¹ · Dhananjaya Kekuda¹ · K. Mohan Rao¹

Received: 12 November 2019 / Accepted: 11 February 2020 / Published online: 21 February 2020
© Springer-Verlag GmbH Germany, part of Springer Nature 2020

Abstract

We report the annealing temperature dependence on the physical properties of TiO₂ (titania) thin films grown using solgel spin-coating method for various concentrations of precursors and stabilizers. X-ray diffraction (XRD) and atomic force microscopy (AFM) images, respectively, provided the structural properties and surface morphology of the films. The XRD results confirm the anatase phase in the films, and a comparative study on morphology has shown that the better uniformity and lower roughness in the films grown at 350 °C compared to films grown at 450 °C for different concentrations. The optical properties of titania thin films were investigated by UV–Vis transmittance and photoluminescence (PL) spectra. All the films exhibited high transmittance, and the indirect bandgap obtained for the films annealed at 350 °C and 450 °C varies between 3.45 and 3.34 eV. The PL spectra provide information regarding defect states in the film for different concentrations. The electrical resistivity of the sample with molar ratio 0.2:0.4 M film decreased for both temperatures compared to other samples.

Keywords Titania films · Annealing temperature · Optical bandgap

1 Introduction

Due to their potential properties, transition metal oxide thin films have attracted many applications in recent years. Among all the transition metal oxides, titanium dioxide or titania (TiO₂) has been used in various fields due to their properties such as transparent conducting nature [1], high refractive index, high dielectric constant, large bandgap with high transmittance, and photocatalytic activity [2, 3]. Being a wide bandgap semiconductor with n-type conducting behavior [4], titania possesses desired electronic properties and excellent physicochemical stability. Thus, it has been widely explored in various applications such as photocatalysts [5], solar cells [6], gas sensors [7], field-effect transistors (FETs) [8], and diodes [9]. Titania has three major crystalline phases, namely anatase, brookite, and rutile. Among these three phases, rutile phase is considered to be thermodynamically stable [10]. The formation of nanostructured titania with different phases depends on the deposition conditions. Many researchers deposited thin

films of titania using various physical and chemical methods such as sputtering [11], chemical vapor deposition [12], SILAR method [13], spray pyrolysis [14], dip coating [15], hydrothermal method [16], and spin coating [17]. Among these, the solgel method provides molecular homogeneity, a wide range of precursor choice, microstructure regulation, the possibility of fine adjustment of end product properties, process flexibility, low-temperature process, and low cost of production [17]. Furthermore, this process can be utilized particularly in deposition of multicomponent oxide layers over common substrate. The properties of titania thin films such as structural, surface morphology, optical, and electrical are dependent on different parameters such as precursor concentration, solvent, stabilizer, viscosity, number of layers, spinning speed, and time, etc. The thickness of the films can be changed by changing viscosity of the final solutions or by changing the spin speed, time, etc. Basri et al. [18] prepared titania thin films using spin-coating method on glass substrate and observed change in structural and electrical properties as a function of annealing temperature in the range 350–500 °C. The crystallite size was found to increase with an increase in annealing temperature and resistivity was decreased due to improved electron mobility and crystallinity. Similarly, Tahir et al. [19] deposited titania thin films on glass substrate using spin-coating method. They observed mixed phase of anatase

✉ K. Mohan Rao
kmohan.rao@manipal.edu

¹ Department of Physics, Manipal Institute of Technology, Manipal Academy of Higher Education, Manipal 576104, India

and rutile as annealing temperature was increased to 800 °C, and conductivity was increased with an increase in annealing temperature. There are other reports available in the literature on heterojunction and gas-sensing property using titania thin films prepared by chemical methods such as spin coating and chemical oxidative polymerization [7, 8]. In the present work, solgel spin-coating technique was used to prepare titania thin films. Also the study of structural, optical, electrical, and photoluminescence properties of the deposited films was carried out with different concentrations of titanium tetraisopropoxide (TTIP) and hydrochloric acid (HCl) annealed at two different temperatures such as 350 °C and 450 °C.

2 Experimental

Titania thin films were deposited by spin-coating unit (Holmarc Model: HO-TH-5) on glass substrates. Before deposition of titania, solgel reaction was carried using titanium tetraisopropoxide (TTIP) (97%, Sigma-Aldrich) as precursor solute and isopropanol (IPA) (99.5%, Merck) as solvent and hydrochloric acid (37%, Merck) as stabilizer. The sol was prepared by adding 0.1:0.4, 0.2:0.4, 0.3:0.4, 0.1:0.7, 0.2:0.7, and 0.3:0.7 molar ratios of TTIP and HCl in 10 ml IPA. This sol was aged for a period of time to attain hydrolysis and condensation reaction. The glass substrates were washed in chromic acid, distilled water, soap solution before coating, and ultrasonicated in IPA for 10 min and dried in a hot air oven for 10 min. A few drops of aged solution were poured on glass substrate and spin-coated with a spinning speed of 1000 rpm for 2 s followed by 3000 rpm for next 30 s. Then each spin-coated layer was preheated on hot plate to evaporate solvent. The films were annealed at 350 °C and 450 °C for 1 h, respectively. The samples deposited with different molar ratios and annealed at 350 °C were coded as T1, T2, T3, T4, T5, and T6 and samples deposited with different molar ratios and annealed at 450 °C were coded as T11, T12, T13, T14, T15, and T16.

The annealed titania samples were characterized using X-ray diffractometer (Rigaku MiniFlex 600) for structural parameters, UV–Vis spectrophotometer (SHIMADZU 1800) and fluorescence spectrophotometer (JASCO FP 8500) for optical properties study, and atomic force microscopy (BRUKER INNOVA SPM) for morphological study, and electrical properties were obtained through van der Pauw methods.

3 Results and discussion

3.1 Structural properties

Figure 1 shows the XRD patterns of titania films annealed at 350 °C and 450 °C for different concentrations of

precursor and stabilizer. The films changed from amorphous to crystalline structure by annealing [2]. The total stress in the films is due to contribution from internal and external stress. One of the contributors for the external stress is the difference in thermal expansion coefficient between glass and the growing thin film. The internal stress is attributed to internal defects such as vacancy and interstitials. At high annealing temperature, the external stress can be minimized, but the internal stress may improve further due to creation of more defects as observed in the present work. In the present work, with an increase in annealing temperature, the disorderness increased marginally as depicted from Urbach energy and PL studies. The results indicate that there is a crystalline anatase phase in the titania films annealed at 350 °C and 450 °C. A low-intense peak of anatase phase (101) was observed even for lower concentration of TTIP. As the concentration of TTIP increased along with suitable concentration of HCl, titania was found to be more crystalline with tetragonal system, and a sharp intense peak corresponding to anatase phase was observed. The anatase phase was further confirmed by comparison of our result with JCPDS file number 21-1272 [6].

Crystallite size (D) of titania thin films of different concentrations annealed at two different temperatures is calculated using Williamson–Hall method [13].

$$\beta \cos \theta = \frac{0.9\lambda}{D} + 4\epsilon \sin \theta \quad (1)$$

where β full width at half maximum (FWHM), λ is wavelength of X-ray used (1.54 Å), ϵ is microstrain and θ is the diffraction angle. Table 1 shows the average size of crystallite for two annealing temperatures calculated using the W–H plots. The high deposition temperature induces an increase in the average size of crystallite due to the migration of grain boundaries [20]. The average crystallite size determined using W–H plot was found to be 50.2 nm for T12 sample annealed at 450 °C. Santosh et al. [21] deposited titania thin films using spray pyrolysis method followed by 2 h of annealing at 500 °C and found crystallite size of ~46 nm calculated through W–H plot. Also, according to Das et al. [8], the spin-coated Ni-doped titania thin films annealed at 450 °C exhibited low crystalline nature. The strain in film is due to lattice mismatch or misfit between the substrate and the growing layer, and it can be quantified by using the following relation [22].

$$\epsilon = \frac{\beta \cos \theta}{4} \quad (2)$$

It is possible to estimate the maximum microstress present in the sample using the relationship.

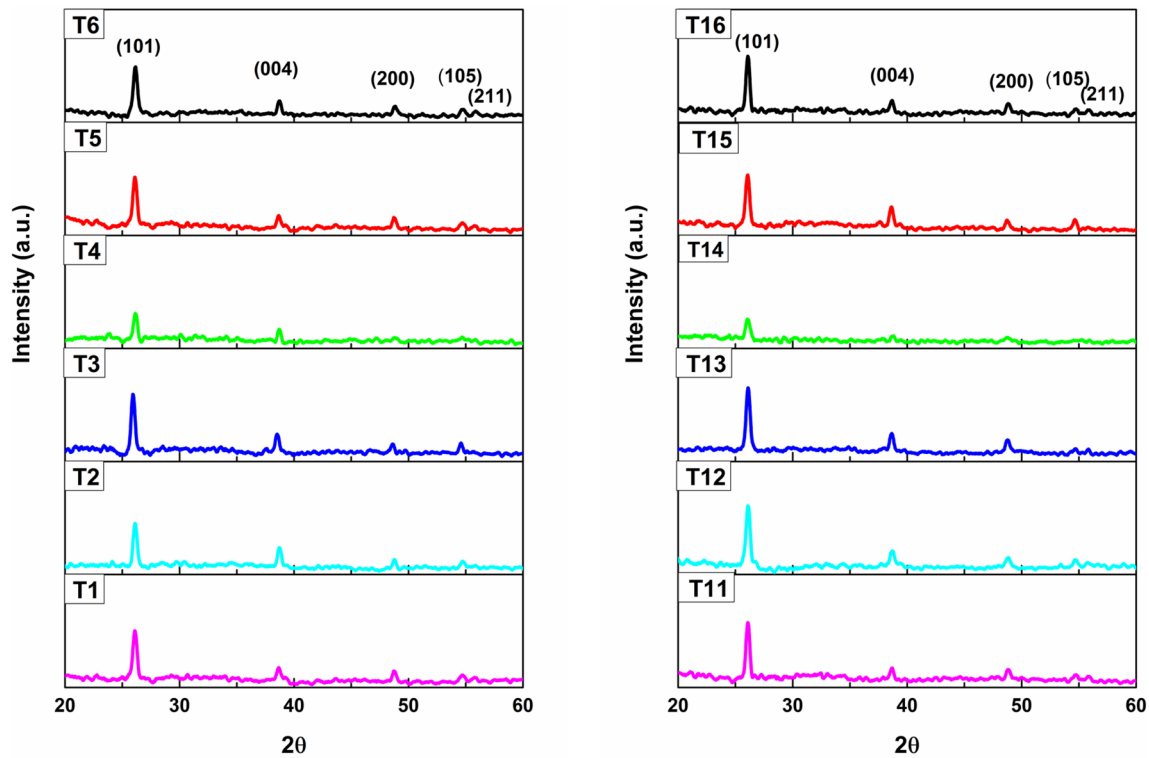


Fig. 1 XRD patterns of titania thin films annealed at 350 °C and 450 °C

Table 1 Structural parameters obtained for titania thin films annealed at 350 °C and 450 °C

Samples	Crystallite size D (nm)	Microstrain $\epsilon \times 10^{-3}$	Microstress σ (GPa)	Dislocation density $\delta \times 10^{15}$	Roughness (nm)
T1	29.9	0.94	0.1328	1.1185	0.308
T2	38.6	0.80	0.1141	0.6697	0.540
T3	24.3	0.37	0.0523	1.6935	0.277
T4	25.0	3.02	0.4280	1.5976	0.267
T5	26.0	0.68	0.0961	1.4788	0.418
T6	28.8	0.65	0.0926	1.2043	0.359
T11	43.7	0.98	0.1385	0.5236	0.679
T12	50.2	1.39	0.1968	0.3968	1.39
T13	32.8	0.76	0.1081	0.9295	0.420
T14	39.4	1.34	0.1898	0.6413	0.353
T15	19.4	0.15	0.0222	2.6389	0.818
T16	28.4	0.60	0.0858	1.2396	0.615

$$\sigma_{\text{stress}} = \frac{\epsilon}{2} E \tag{3}$$

where $E=282.76$ GPa for titania, E represent Young’s modulus of the material [23].

The crystallite size has an inverse relation to FWHM of the diffraction peak. The FWHM of the diffraction peak in thin films is very sensitive to the effect of stress/strain due to constraint imposed by the substrate during annealing.

Strain in thin film induces broadness in the diffraction peak, which in turn leads to the reduction in the grain size. The effect of the strain due to substrate prevails up to the critical thickness, above which the deposited material behaves normal polycrystalline nature.

Dislocation density is known as dislocation line length per crystal unit volume. This provides information about crystal structure such as crystal imperfection in one

position of the crystal in relation to another [24]. It is mathematically expressed as

$$\delta = \frac{1}{D^2} \tag{4}$$

From Table 1, it is clear that an increase in the size of crystallite with a decrease in strain and dislocation density increases the crystallinity of titania thin film. The reduction in strain suggests a decrease in the concentration of imperfections of lattices and the production of high-quality films [6] (Fig. 2).

3.2 Morphological study

Three-dimensional images of the surface topography of titania thin films of different concentrations annealed at different temperatures are shown in Fig. 3. The roughness obtained for films annealed at both temperatures is given in Table 2. The rise in annealing temperature helps the marginal grain growth and an increase in roughness of

films. The uneven surfaces developed at high temperature are believed to be due to the coalescence of particles on the surface of the film. The parameters of roughness such as mean roughness (R_a) and mean-root-square roughness (R_q) are used by statistical method to quantify surface roughness. In this case, one more factor, i.e., stabilizer concentration, also brings changes in the morphology of the titania thin films. Being a strong oxidative and weak reductive agent, HCl at suitable concentrations may bring agglomeration of grains. An increase in grain size as result of agglomeration improves the roughness of the film at high-temperature annealing for all samples except T14 because higher concentration of HCl causes low crystallinity and low roughness due to high acidic nature of solution. The roughness obtained in the present work was 1.39 nm for T12 annealed at 450 °C. According to Garcia et al. [25], the roughness was found to be 1.70 nm for the titania films annealed at 700 °C. Hence, both temperature-induced agglomeration and agglomeration due to stabilizer may violate roughness of the film.

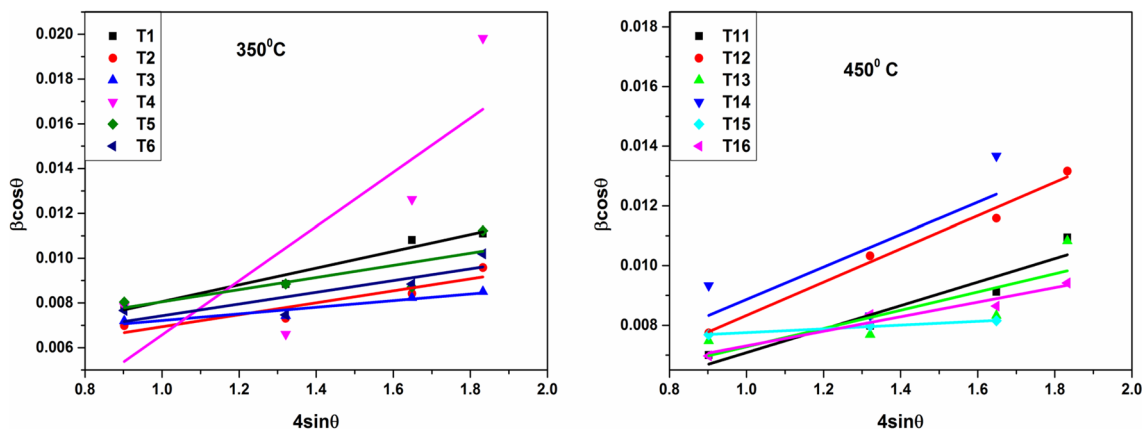


Fig. 2 W–H plots for titania thin films annealed at 350 °C and 450 °C

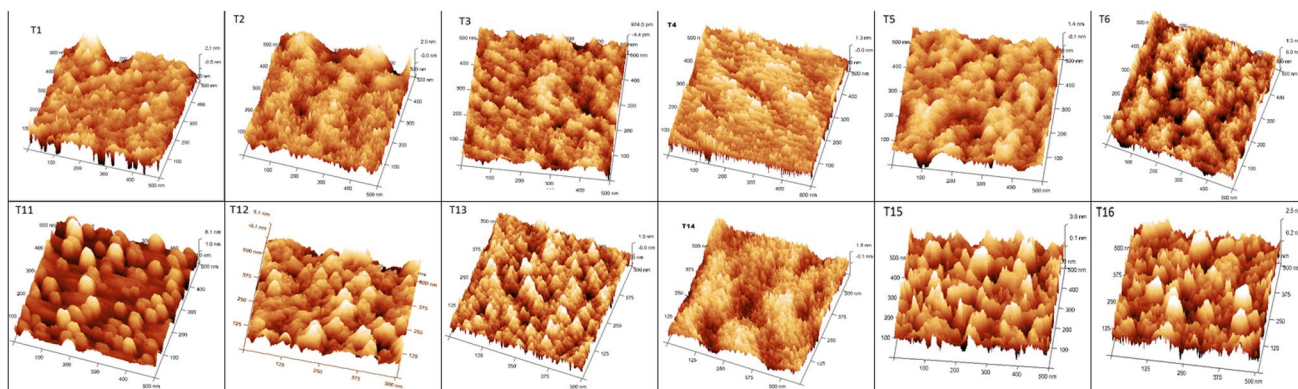


Fig. 3 AFM images of titania thin films annealed at 350 °C and 450 °C

Table 2 Optical parameters of titania thin films annealed at 350 °C and 450 °C

Sample	Thickness using profilometer (nm)	Thickness using Swanepoel method (nm)	Optical bandgap (eV)	Refractive index	Urbach Energy (meV)
T1	293	295	3.46	2.56	138
T2	370	393	3.40	2.69	148
T3	377	368	3.37	2.64	146
T4	215	282	3.45	2.59	136
T5	347	456	3.44	2.59	142
T6	360	341	3.39	2.60	145
T11	362	341	3.45	2.65	144
T12	414	393	3.34	2.59	152
T13	333	394	3.36	2.65	146
T14	283	302	3.45	2.58	136
T15	342	488	3.43	2.60	141
T16	412	411	3.41	2.59	150

3.3 Optical study

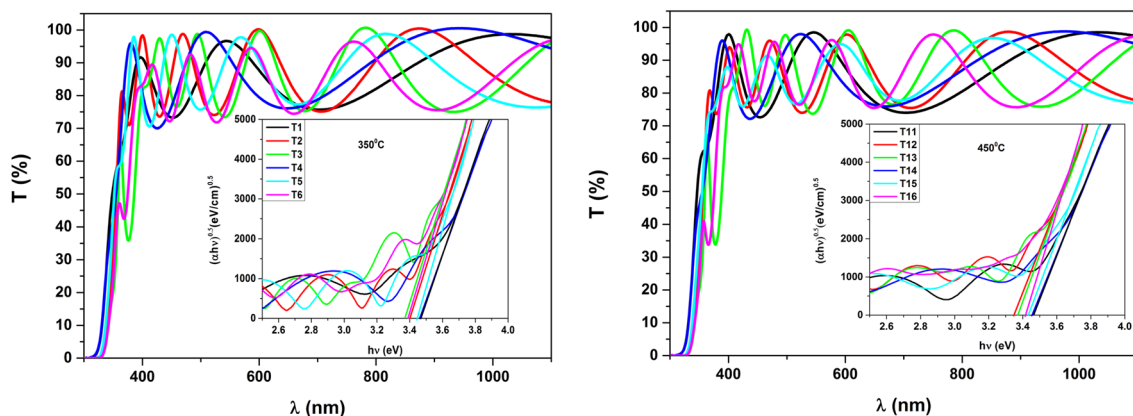
Figure 4 displays the optical transmission spectrum of annealed titania thin films. The spectrum exhibited oscillatory behavior that was formed at the air/metal oxide/substrate interfaces due to interference effects. The average optical transmittance of the films as seen from the graph is about 95–98%. High transmittance of the films is due to the crystalline nature of the films, which is evident from XRD results. The grown multilayer structure exhibited multiple optical interference fringes caused by slight difference in refractive indices of layers and between film and substrate. It is also noticed that the color of these films changes as the number of layers increases [14].

Titania thin films with anatase phase correspond to indirect bandgap nature [26]. In general, optical bandgap of titania thin films deposited at different temperatures are determined using following mathematical expression:

$$(\alpha h\nu) = A(h\nu - E)^n \quad (5)$$

where α is a coefficient of absorption, A is a constant for indirect transition, $h\nu$ is an incident photon energy, E is a material optical bandgap, and $n=0.5$ for indirect bandgap semiconductor transition [27]. In general, absorption edge provides an estimate of the obtained bandgap of a thin film. The observed optical bandgap marginally reduced with an increase in annealing temperature to 450 °C. The optical bandgap obtained for all the titania samples of different concentration vary between 3.45 and 3.34 eV. Wang et al. [28] reported that titania prepared using spin coating produces an optical indirect bandgap of about 3.49 eV for films annealed at 700 °C for 2 h.

The coefficient of extinction is an imaginary component of the refraction index and is related to the coefficient of absorption which gives the amount of light attenuated as light passes through material. It is denoted by k , and a

**Fig. 4** Transmission spectra of titania thin films with optical bandgap (inset) annealed at 350 °C and 450 °C

positive k value indicates that the light is absorbed by system, and if $k=0$, the light passes without any loss in the system.

$$k = \frac{\alpha \lambda}{4\pi} \tag{6}$$

where α is the coefficient of absorption and λ is the wavelength of light used. The rise and fall in the extinction coefficient of titania thin film at different temperatures is due to the absorption of light by particles of various sizes and shapes [6].

The transition of electrons from the top of the valance band to the bottom of the conduction band takes place due to optical absorption near the edges of the band. This process is more efficient when photon energy is greater than optical bandgap, even though small absorption may be observed due to the presence of sub-bands which use photon energy smaller than bandgap. If these electrons experience a disturbance, this induces a density of their state $\rho(h\nu)$, where $h\nu$ is photon energy tailing into energy gap. This tail extending into the optical bandgap is known as Urbach tail, and therefore, the absorption coefficient also decreases exponentially, and the corresponding energy is referred to as Urbach energy and measured using the following formula [13]

$$\alpha = \alpha_0 \exp \frac{E_g}{E_u} \tag{7}$$

where α is a coefficient of absorption, α_0 is a constant, $E_g = h\nu$ is an optical bandgap, and E_u is an Urbach energy. As shown in Fig. 5, the graph of $\ln \alpha$ versus $h\nu$ is plotted. This graph's reciprocal slope yields Urbach energy [29, 30].

The Urbach energy corresponding to different samples annealed at 350 °C and 450 °C are shown in Table 2. The sample T12 and T16 shows higher E_u which may be

attributed to increase in oxygen vacancy created at high-temperature annealing.

In summary, the optical bandgap obtained for T12 sample in the present work is less in comparison with reported values using different methods [17, 23]. The Urbach energy obtained in the present work is high for T12 due to oxygen-related defects. The similar results were reported [17, 31] where increase in Urbach energy is related to defects such as oxygen vacancy.

3.4 Photoluminescence (PL) study

The study of photoluminescence can provide information on the different processes of recombination and the material's catalytic activity. Figure 6 shows the titania thin-film PL spectra. These were recorded in the wavelength range from 350 to 600 nm with 330 nm as excitation wavelength for titania films annealed at 350 °C and 450 °C. These spectra show two weak bands and one strong band. The strong band between 350 and 400 nm corresponds to the transition from the valance band to the conduction band, and the energy corresponding to this wavelength range is the titania optical bandgap. The other two weak bands over 400 nm are due to defects linked to oxygen vacancy and surface defects. The typical spectra of photoluminescence originate due to self-trapped excitons, oxygen vacancies, and surface defects [6]. The broad band transition may result from radiative combination which is either electron trapping or hole trapping [32]. The spectrum of wavelengths from 400 to 500 nm refers to defect related to oxygen vacancy. The profile of the PL obtained with different peak positions were also observed by Garcia et al. [25] with blue and green emission assigned to oxygen vacancy. According to Arunachalam et al. [23], the peak between 400 and 500 nm are strongly associated with oxygen vacancy.

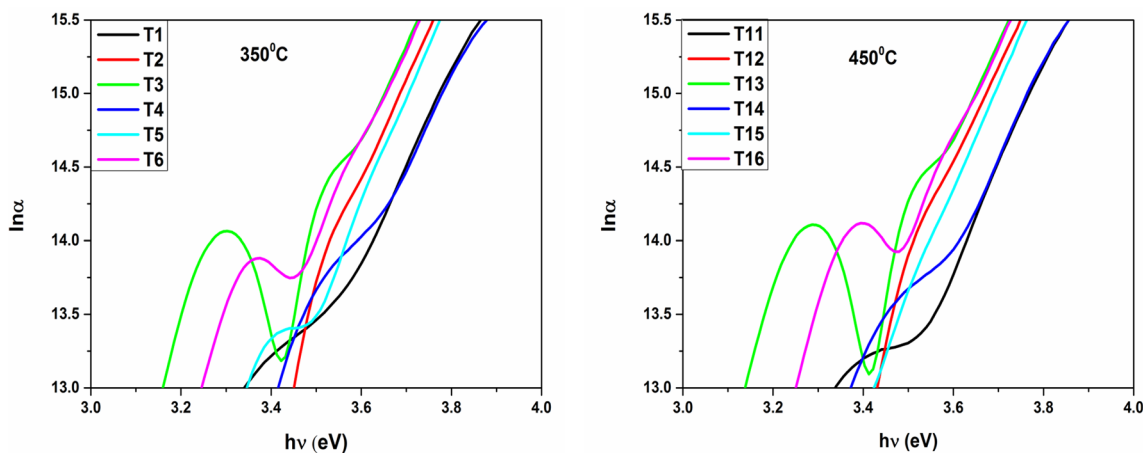
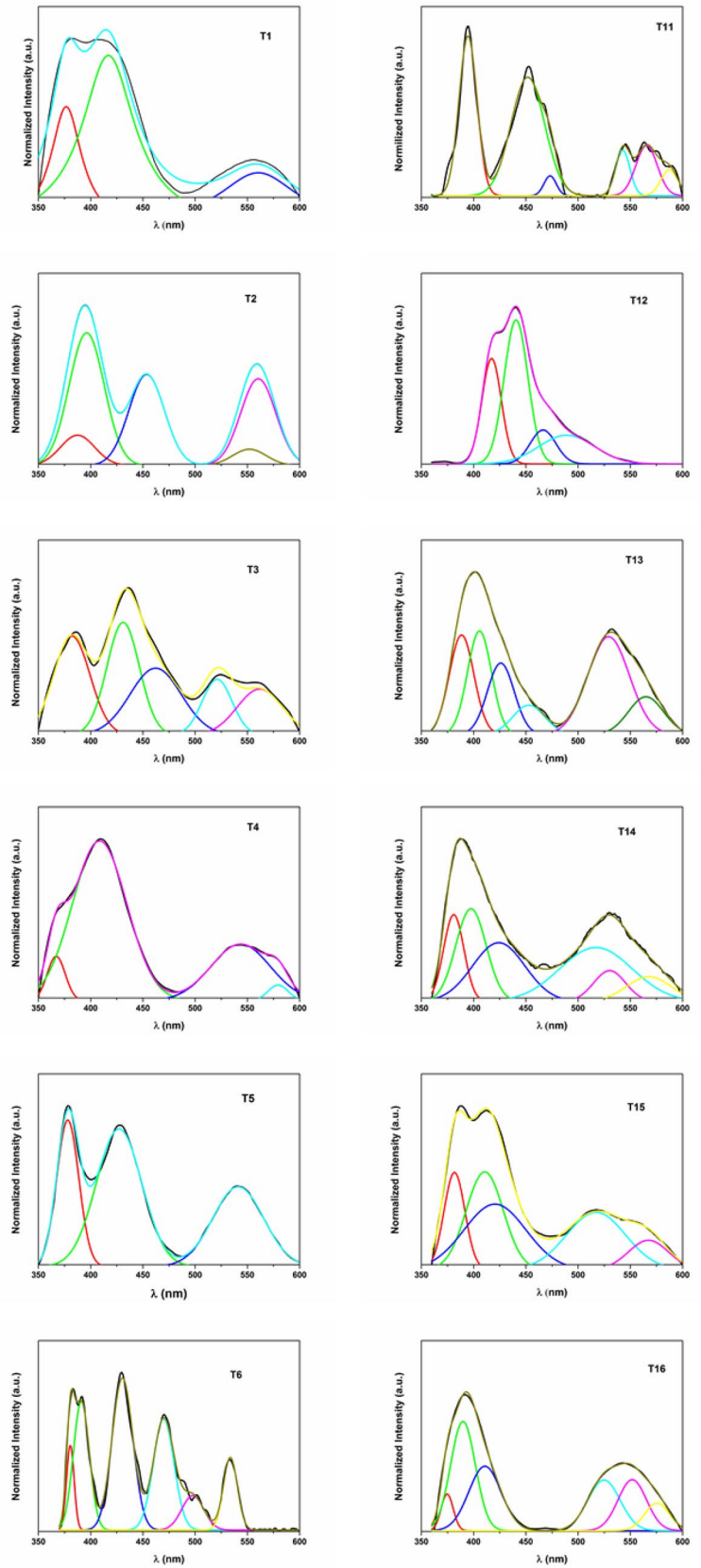


Fig. 5 Urbach plot for titania thin films annealed at 350 °C and 450 °C

Fig. 6 Photoluminescence spectra of titania thin films annealed at 350 °C and 450 °C



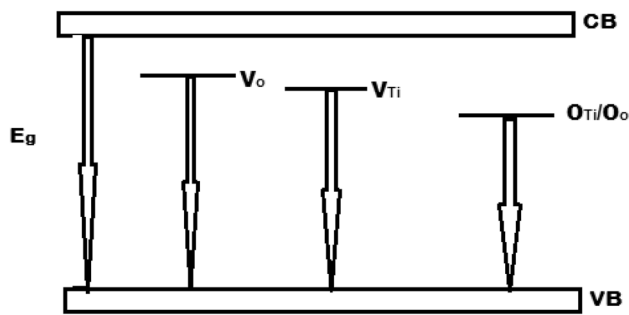


Fig. 7 Schematic representation of energy-level diagram for titania

The oxygen vacancies are intrinsic defects in titania lattice and form intermediate energy levels within titania bandgap introducing several recombination centers of photoinduced electrons and holes, or this may be due to the recombination process of donor acceptors or the transition from conductive band to oxygen antisites [6]. The wavelength range from 500 to 600 nm corresponds to surface defects [33].

Figure 7 shows energy-level diagram for titania thin film involving defect levels. As mentioned above, oxygen vacancies contributing for low bandgap and also titanium vacancies are inline to contribute lower bandgap. Some surface defects including interstitials and antisites (O_{Ti}/O_o) often cause a transition from the conduction band (CB) to the valance band (VB) by lying just below the conduction band.

At these two annealing temperatures, the positions of strong band and weak bands are shifted. At 350 °C, positions of T1–T6 were observed at higher wavelength side. However, for films annealed at 450 °C, labeled as T11–T16, the peak positions shifted to lower wavelength side. For all these concentrations, there are three broad regions as aforementioned corresponding to band edge transition, oxygen vacancies, and surface defects except for T12. The most intense peak appeared as strong band without any weak bands due to shallow trap states originated from oxygen vacancies associated with Ti^{3+} . Several small peaks were observed in rest of the samples due to self-trapped excitons. These self-trap exciton cause loss of excitation energy through lattice relaxation [34, 35].

3.5 Electrical study

Figure 8 shows electrical resistivity of titania thin films. The resistivity of films was measured at room temperature by using van der Pauw method. The decrement of resistivity at high annealing temperature might be contributed to few factors. One of them might be an increase in the crystallinity with annealing temperature, and another one is oxygen vacancy. Resistivity of the film decreases with annealing temperature indicating the behavior of n-type

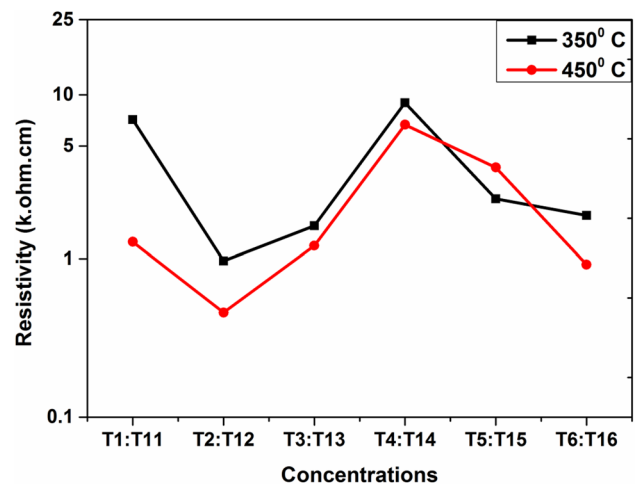


Fig. 8 Resistivity of titania thin films annealed at 350 °C and 450 °C

conductivity [28]. The XRD results for sample T12 have shown an increase in grain size with reduction in dislocation density and hence provide higher region of orderness and reduce scattering probabilities [29]. The addition of stabilizer in proportion with TTIP causes improvement in the oxygen vacancy since Urbach energy is more for T12 and T16. For T4 and T14, lower concentration of precursor and higher concentration of stabilizer leads to more acidic solution. This acidic solution reduces crystallinity of the titania film and quenches the PL emission. Because of this reason, reduced conductivity or higher resistivity for T4 and T14 was observed. The electrical resistivity values obtained in the present study are lower in comparison with those obtained by Sta et al. [17]. However, electrical resistivity values are found to be in the same order as reported by others using different methods for deposition [18, 23]. As these oxygen vacancies act as donor impurities and provide n-type doping to the material, they are more efficient in optical absorption and can be used for device applications [36].

4 Conclusion

The titania thin films were prepared using spin coating by varying TTIP concentration and HCl annealed at 350 °C and 450 °C, respectively. The phase identification and crystallinity of the samples were analyzed through XRD results. A crystalline anatase phase was observed for the films grown at different precursor and stabilizer concentrations. The surface morphology studies through atomic force microscopy (AFM) evidenced a slight increase in roughness for high-temperature annealing. Optical properties of the films showed high transmittance and reduced bandgap for the sample annealed at 450 °C, and Urbach energy obtained for sample T12 and T16 was more due to increment in the

oxygen-related defects. The photoluminescence study provides information regarding weak band region corresponding to oxygen vacancy and other surface defects. The sample T12 showed lower resistivity due to increased grain size and oxygen vacancies.

Acknowledgements The authors thank Dr. Sudha Kamath for providing photoluminescence spectrophotometer facility and central Instrumentation facility (CIF) Manipal Institute of Technology, Manipal Academy of Higher Education, Manipal, for other characterization facilities and financial support.

References

- J. Gao, K. Kempa, M. Giersig, E.M. Akinoglu, B. Han, R. Li, *Adv. Phys.* **65**, 553 (2016)
- A. Elfanaoui, E. Elhamri, L. Boulkaddat, A. Ihlal, K. Bouabid, L. Laanab, A. Taleb, X. Portier, *Int. J. Hydrogen Energy* **36**, 4130 (2011)
- M.B. Tahir, K. Nadeem, M. Hafeez, S. Firdous, *Indian J. Pure Appl. Phys.* **55**, 716 (2017)
- M.K. Nowotny, P. Bogdanoff, T. Dittrich, S. Fiechter, A. Fujishima, H. Tributsch, *Mater. Lett.* **64**, 928 (2010)
- A. Di Paola, M. Bellardita, L. Palmisano, *Catalyst* **3**, 36 (2013)
- A. Arunachalam, S. Dhanapandian, C. Manoharan, R. Sridhar, *Spectrochim Acta Part A Mol. Biomol. Spectrosc.* **149**, 904 (2015)
- S. Srivastava, S. Kumar, V.N. Singh, M. Singh, Y.K. Vijay, *Int. J. Hydrogen Energy* **36**, 6343 (2011)
- S. Das, D. Liu, J.B. Park, Y.B. Hahn, *J. Alloys Compd.* **553**, 188 (2013)
- J. Meyer, S. Hamwi, M. Kröger, W. Kowalsky, T. Riedl, A. Kahn, *Adv. Mater.* **24**, 5408 (2012)
- A.S. Bhatti, I. Rehan, S. Sultana, N. Khan, Z. Qamar, K. Rehan, *Mater. Res. Express* **3**, 1 (2016)
- M. Sreedhar, I. Neelakanta Reddy, C.V. Reddy, J. Shim, J. Brijitta, *Mater. Sci. Semicond. Process.* **85**, 113 (2018)
- H. Rasoulnezhad, G. Kavei, K. Ahmadi, M.R. Rahimpour, *Appl. Surf. Sci.* **408**, 1 (2017)
- V.K. Ashith, G.K. Rao, R. Smitha, S.N. Moger, *Ceram. Int.* **44**, 17623 (2018)
- M. Dudita, L.M. Mancieru, M. Anastasescu, M. Nicolescu, M. Gartner, A. Duta, *Ceram. Int.* **40**, 3903 (2014)
- R. Pandeewari, R.K. Karn, B.G. Jeyaprakash, *Sens. Actuators B Chem.* **194**, 470 (2014)
- V.R. Bandi, C.M. Raghavan, B.K. Grandhe, S.S. Kim, K. Jang, D.S. Shin, S.S. Yi, J.H. Jeong, *Thin Solid Films* **547**, 207 (2013)
- I. Sta, M. Jlassi, M. Hajji, M.F. Boujmil, R. Jerbi, M. Kandyla, M. Kompitsas, *J. Sol-Gel. Sci. Technol.* **421**, 1 (2014)
- M. Basri, M.N. Asiah, M.K. bin Ahmad, M.H. Mamat, M. Rusop Mahmood, *Adv. Mater. Res.* **667**, 371 (2013)
- M.B. Tahir, S. Hajra, N.R. Khalid, M. Rizwan, G.N. Watto, *J. Inorg. Organomet. Polym. Mater.* **28**, 1 (2018)
- S. Aksoy, Y. Caglar, *J. Alloys Compd.* **613**, 330 (2014)
- M.V. Santhosh, D.R. Deepu, R. Geethu, K. Rajeev Kumar, C. Sudha Kartha, K.P. Vijayakumar, *Semicond. Sci. Technol.* **29**, 115026 (2014)
- H.A. Yurtsever, M. Çiftçiöglü, *J. Alloys Compd.* **695**, 1336 (2017)
- A. Arunachalam, S. Dhanapandian, C. Manoharan, G. Sivakumar, *Spectrochim Acta Part A Mol. Biomol. Spectrosc.* **138**, 105 (2015)
- A. Moses Ezhil Raj, V. Agnes, V. Bena Jothy, C. Sanjeeviraja, *Mater. Sci. Semicond. Process.* **13**, 389 (2010)
- L.M.P. Garcia, M.T.S. Tavares, N.F. Andrade Neto, R.M. Nascimento, C.A. Paskocimas, E. Longo, M.R.D. Bomio, F.V. Motta, *J. Mater. Sci. Mater. Electron.* **29**, 6530 (2018)
- M.R. Golobostanfard, H. Abdizadeh, *Ceram. Int.* **38**, 5843 (2012)
- F. Bensouici, M. Bououdina, A.A. Dakhel, T. Souier, R. Tala-Ighil, M. Toubane, A. Iratni, S. Liu, W. Cai, *Thin Solid Films* **616**, 655 (2016)
- G.Q. Wang, W. Lan, M.L. Yu, G.J. Han, Y. Wang, Q. Su, X.Q. Liu, *J. Mater. Sci. Mater. Electron.* **22**, 463 (2011)
- D. Komaraiah, P. Madhukar, Y. Vijayakumar, M.V. Ramana Reddy, R. Sayanna, *Mater. Today Proc.* **3**, 3770 (2016)
- J. Yang, Y. Hu, C. Jin, L. Zhuge, X. Wu, *Thin Solid Films* **637**, 9 (2017)
- K.H. Rahman, A.K. Kar, *Mater. Res. Express* **6**, 096436 (2014)
- K. Kawamura, N. Suzuki, T. Inoue, T. Okumura, Y. Shimazu, T. Okumura, *J. Phys. Conf. Ser.* **995**, 012067 (2018)
- T.S. Senthil, N. Muthukumarasamy, S. Agilan, M. Thambidurai, K.V.R. Murthy, R. Balasundaraprabhu, *Bull. Kor. Chem. Soc.* **11**, 831 (2009)
- M. Fallah, R. Rahimi, M. Rabbani, *Appl. Surf. Sci.* **316**, 456 (2014)
- M.I. Khan, K.A. Bhatti, R. Qindeel, H.S. Althobaiti, N. Alonizan, *Results Phys.* **7**, 1437 (2017)
- B. Bharti, S. Kumar, H.N. Lee, R. Kumar, *Sci. Rep.* **6**, 1 (2016)

Publisher's Note Springer Nature remains neutral with regard to jurisdictional claims in published maps and institutional affiliations.